

Origin of Enhanced Dielectric Tunability in Antiferroelectric Ceramic Systems

Vida Jurečič, Tadej Rojac, Vid Bobnar, and Nikola Novak*

Antiferroelectric ceramics are considered as highly promising materials for the development of novel DC-link, snubber, and filter capacitors used in high-power and high-speed electronics for electromotive and renewable energy applications, medical equipment, and weapons platforms. In particular, the increase of the dielectric permittivity with bias electric field, i.e., the dielectric tunability, is one of the most interesting and still not fully understood properties of antiferroelectric materials. The in situ dielectric measurements and thermometry of $\text{Pb}_{0.99}\text{Nb}_{0.02}[(\text{Zr}_{0.57}\text{Sn}_{0.43})_{0.92}\text{Ti}_{0.08}]_{0.98}\text{O}_3$ ceramics reveal that the dielectric response increases with bias electric field in the antiferroelectric phase due to the non-linear contributions, most likely originating in the irreversible domain wall motions. Furthermore, extraordinarily high values of the dielectric tunability ($\approx 375\%$) and the figure of merit ($\approx 1680\%$) are determined at the temperature of the triple point. The minimization of the domain size near the triple point is proposed to be responsible for the enhanced dielectric tunability. The proposed mechanism is supported by the enhanced irreversible Rayleigh coefficient and via observation of minimized domains by piezoresponse force microscopy. The exploration of the role of the domain structure in antiferroelectrics contributes to a better understanding of their unique dielectric properties and opens a new possibility for the development of high-performance capacitors.

materials are widely used in electronic devices and integrated circuits as wavelet filters, lens antennae, tunable oscillators, phase shifters, and varactors in microwave devices.^[1–3] So far, ferroelectric materials have been considered ideal candidates for tunable microwave devices if operated above the Curie temperature. In the paraelectric (PE) phase, the anisotropy superiority of the dielectric permittivity in the ferroelectric state is ignored at the expense of reduced dielectric tunability, while the absence of the domain structure strongly decreases dielectric losses and promotes non-hysteresis behavior of dielectric permittivity.^[1,4,5] In contrast to ferroelectric (FE) materials, antiferroelectric (AFE) materials in their antiferroelectric state exhibit an increase of dielectric permittivity with increasing electric field and low dielectric losses due to the reduced AFE domain dynamic. Moreover, their operating temperature range can easily exceed 150 °C. As a result, they can operate sustainably under electric bias, high AC ripple currents, or in harsh thermal environments.^[2,6,7] These are important

parameters for capacitors used in high-power electronics applications, such as snubbers, DC-links, and filter capacitors used in the engine control unit in electric cars and power inverters.

Antiferroelectricity is characterized by the double hysteresis loop which is a consequence of the reversible electric field-induced phase transition between the macroscopically non-polar AFE and polar FE phase. The polar instability at the field-induced phase transition is often considered the origin of antiferroelectric's peculiar electrical,^[8,9] thermal,^[10] and mechanical^[11] properties. Despite their promising dielectric behavior under the external bias field, only a few studies on the dielectric tunability of antiferroelectrics can be found.^[9,12–19] Most works investigate the relationship between dielectric tunability and field-induced phase transition or chemical modification. Pan et al. demonstrated that dielectric tunability in antiferroelectric PbZrO_3 can be adjusted or converted between the classical ferroelectric and antiferroelectric one by controlling the concentration of adatom bombardment-induced defects.^[18] Moreover, a strong enhancement of the dielectric tunability of $\approx 220\%$ in an antiferroelectric $\text{Pb}(\text{Nb},\text{Zr},\text{Sn},\text{Ti})\text{O}_3$ system was related to the critical behavior of the field-induced antiferroelectric to paraelectric phase transition.^[19]

1. Introduction

Dielectric tunability describes the dielectric permittivity change under an externally applied bias electric field. Tunable dielectric

V. Jurečič, V. Bobnar, N. Novak
Condensed Matter Physics Department
Jožef Stefan Institute
Ljubljana SI-1000, Slovenia
E-mail: nikola.novak@ijs.si

V. Jurečič, T. Rojac, V. Bobnar
Jožef Stefan International Postgraduate School
Ljubljana SI-1000, Slovenia
T. Rojac
Electronic Ceramics Department
Jožef Stefan Institute
Ljubljana SI-1000, Slovenia

 The ORCID identification number(s) for the author(s) of this article can be found under <https://doi.org/10.1002/adfm.202412739>

© 2024 The Author(s). Advanced Functional Materials published by Wiley-VCH GmbH. This is an open access article under the terms of the [Creative Commons Attribution](https://creativecommons.org/licenses/by/4.0/) License, which permits use, distribution and reproduction in any medium, provided the original work is properly cited.

DOI: 10.1002/adfm.202412739

The dielectric response of ferroelectrics consists of intrinsic and extrinsic contributions. The intrinsic contributions are related to lattice deformation under applied subswitching electric fields. In contrast, the extrinsic contributions refer to the movements of interfaces in the material, e.g., phase boundaries and/or domain walls.^[20,21] Hence, the reduction of the dielectric permittivity under the biased electric field in the ferroelectric phase is a consequence of the reduced domain dynamic and/or saturation of polarization,^[22,23] while the dielectric tunability in the paraelectric phase was attributed to the hardening of the phonon mode.^[24] Whereas the dielectric tunability and its enhancement in ferroelectric materials have been widely investigated and are well understood, considerably less attention has been given to antiferroelectrics. He and Tan investigated the incommensurate modulation under an electric field in antiferroelectric ceramics $\text{Pb}(\text{Nb},\text{Zr},\text{Sn},\text{Ti})\text{O}_3$. They concluded that before the field-induced phase transition, an alignment of Pb-cations of which the displacement vector is nearly parallel with the electric field vector takes place. The aligning process of Pb-cations involves a 180°-domain switching-like process.^[25] The alignment of Pb-cations indicates that the domain pattern in AFE changes under an electric field. This was demonstrated by Vakhrushev et al. who experimentally and theoretically showed that an external electric field can manipulate AFE domains.^[26] Hence, the question arises, whether the increase of the dielectric permittivity under the electric bias field is due to the free energy instability at the field-induced phase transition or a result of domain rearrangement in the AFE phase.

Here, by employing in situ dielectric measurements and thermometry at different electric fields with different superimposed AC signals and various temperatures, the origin of the increased dielectric permittivity under an electric bias field in an antiferroelectric $\text{Pb}_{0.99}\text{Nb}_{0.02}[(\text{Zr}_{0.57}\text{Sn}_{0.43})_{0.92}\text{Ti}_{0.08}]_{0.98}\text{O}_3$ (abbreviated as PNZST) ceramic is studied. Results revealed the increase in the dielectric permittivity under the electric field before the field-induced AFE-FE phase transition. This indicates that the origin of the increased dielectric permittivity under the electric field is most likely due to the contribution of the AFE domains. Furthermore, the dielectric tunability maximum exhibits a strong AC signal dependency, i.e., the temperature of the dielectric tunability maximum is shifted from AFE-PE critical end point temperature toward the FE, AFE, and PE coexistence temperature with an increase in dielectric tunability from ≈ 200 to 375%. The strong enhancement in tunability at the coexistence point is associated with the minimization of domain structures and consequently, enhanced domain contribution indicated by dielectric Rayleigh-type analysis and piezoresponse force microscopy measurements.

2. Results and Discussion

The room temperature X-ray diffraction pattern and scanning electron microscopy (SEM) micrograph (see Figures S1 and S2, Supporting Information) suggest the existence of a pure perovskite phase with no evidence of secondary phases. The X-ray diffraction pattern of antiferroelectric PNZST ceramics matches the previously reported data in the literature.^[11,27] The examination of the SEM micrograph confirms the high density of the pre-

pared ceramics with relatively uniform grain distribution. The investigated composition of the antiferroelectric PNZST ceramics is characterized by the ferroelectric $\xrightarrow{\approx 297\text{ K}}$ antiferroelectric $\xrightarrow{\approx 408\text{ K}}$ paraelectric phase sequence as shown in Figure S3 (Supporting Information). The temperature-dependent dielectric permittivity under various applied electric fields demonstrates that the phase transition temperatures as well as the nature of the phase transition can be altered by an external electric field which consequently affects the functional properties, such as electrical, mechanical, and thermal properties.^[19] Therefore, dielectric hysteresis loops and thermometry under isothermal conditions were simultaneously performed on annealed antiferroelectric PNZST ceramics. **Figure 1a** shows the dielectric response and sample temperature change (ΔT_{sample}) as a function of an externally applied electric field. At 343 K, the PNZST ceramics exhibit an antiferroelectric behavior with zero macroscopic polarization. The electric field evolution of the dielectric permittivity depicts the expected antiferroelectric-like response with increasing dielectric permittivity at lower electric fields. At and above the field-induced AFE-FE phase transition an expected ferroelectric response is observed with a sharp reduction in the dielectric permittivity. The four peaks in the dielectric response reveal the reversibility of the field-induced AFE-FE phase transition. Concomitantly with the dielectric response, the sample temperature as a function of the electric field was also traced. The sample temperature response shows two positive and two negative temperature changes, which are associated with the release and absorption of the latent heat at the first-order field-induced phase transitions.^[19,28] The high-resolution temperature measurement shows a small temperature difference of ≈ 33 mK between the positive and negative temperature changes of the sample. The difference could be attributed to the additional heating at the AFE-FE phase transition, originating from the domain wall switching of the FE phase.^[2,29,30]

A more detailed insight into the dielectric and temperature response under the applied electric field is shown in Figure 1b,c. Figure 1b depicts the response of the dielectric permittivity and sample temperature obtained in the first quarter of the electric field cycle. The dielectric permittivity remains nearly constant at electric fields up to $\approx 10\text{ kV cm}^{-1}$. However, above 10 kV cm^{-1} , the dielectric response nonlinearly increases and reaches the maximum value at the critical electric field at which the FE phase is induced. The increase of the dielectric permittivity in the antiferroelectric phase could be attributed to the transition instability and divergent nature of the dielectric permittivity at the field-induced first-order phase transition. On the other hand, the sample temperature remains constant up to the critical field of the phase transition which indicates no release of latent heat due to the pre-transition effects of the field-induced phase transition. The imaginary part of the dielectric constant, ϵ'' , determines the energy loss per unit volume in the material, which is in ferroelectric materials, at least in part, related to the domain switching.^[2,29] The electric field evolution of ϵ'' exhibits similar behavior as the dielectric permittivity (see Figure 1c). Low ϵ'' values (5 at zero electric field and 25 just before the AFE-FE transition correspond to low dielectric losses, $\tan\delta = \epsilon''/\epsilon'$, of ≈ 0.004 and ≈ 0.018 , respectively) indicate the minimized domain activity and negligible heat losses in the antiferroelectric phase. However, by increasing the

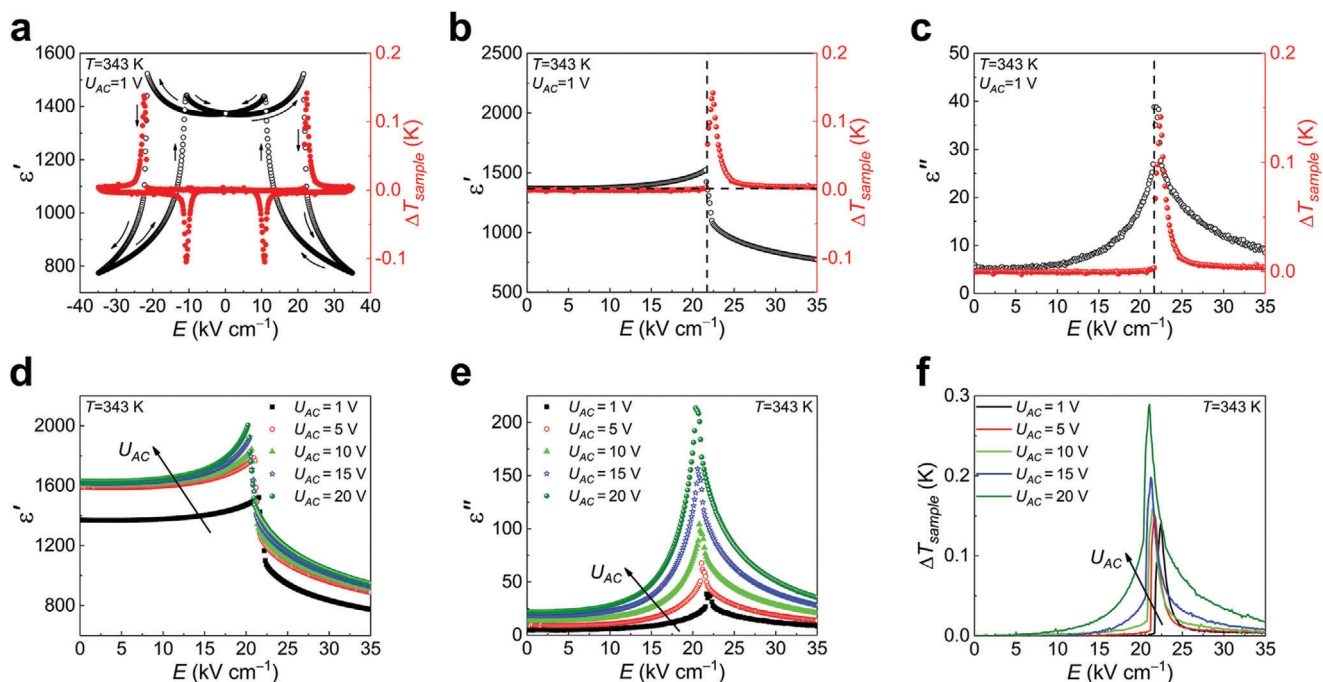


Figure 1. a) Dielectric and temperature measurements as a function of the DC electric field during the second measurement loop at 343 K, 1 V AC signal, and 10 kHz. b,c) A detailed view of the dielectric permittivity, the imaginary part of the dielectric constant, and sample temperature obtained in the first quarter of the electric field cycle. Comparison of d) dielectric permittivity, e) dielectric losses, and f) sample temperature change measured with different AC signals.

magnitude of the superimposed AC voltage from 1 to 20 V, the dielectric permittivity increases. The range of the constant ϵ' (below bias fields of $\approx 10 \text{ kV cm}^{-1}$) decreases with increasing AC signal as the nonlinear contribution to the dielectric response becomes more pronounced (see Figure 1d). ϵ'' shows the same dependency with increasing AC signal as ϵ' . The increase of the ϵ' magnitude and nonlinearity of the system, as well as the increase of ϵ'' indicate the increase of the extrinsic contributions, which, according to the basic Rayleigh relations, should be irreversible. This is corroborated by the sample temperature response as a function of the electric bias field obtained at various AC signals (Figure 1f). The sample temperature change (ΔT_{sample}) increases with increasing AC signal in the antiferroelectric phase which could be due to the irreversible domain wall contribution and generated heat related with it. Hence, the in situ dielectric and thermometry results demonstrated that the increase of the dielectric permittivity in the antiferroelectric phase under an external electric field is related to hysteretic non-linear processes, most likely to the irreversible domain wall contribution. Therefore, to identify the influence of the domain wall contributions on the dielectric tunability, the dielectric response was measured as a function of the electric field at different temperatures and AC signals.

Since the dielectric permittivity increases with the electric field in the antiferroelectric phase, the dielectric tunability, η , of an AFE can be calculated as follows:^[1,5]

$$\eta = \frac{\epsilon'_{\text{max}}(E) - \epsilon'(E=0)}{\epsilon'(E=0)} \times 100\% \quad (1)$$

where $\epsilon'_{\text{max}}(E)$ and $\epsilon'(E=0)$ are the maximum dielectric permittivity of the antiferroelectric phase at the electric field E and dielectric permittivity at zero electric field, respectively. Another important parameter of the dielectric tunability is the figure of merit, FOM , defined as the ratio between the dielectric tunability and the dielectric losses:^[31,32]

$$FOM = \frac{\eta}{\tan\delta} \quad (2)$$

Figure 2a–c shows the dielectric permittivity as a function of the external electric field at 388 K for three different AC signals; 1, 10, and 20 V, respectively. At 388 K and 1 V AC signal, the dielectric permittivity changes for ≈ 3136 when the bias electric field is changed from zero to critical electric field which is much larger compared to ϵ' change of ≈ 152 at 340 K. The dielectric permittivity change is further enhanced by increasing the AC signal. At 20 V signal, ϵ' changes for ≈ 8182 at 388 K and only for ≈ 373 at 340 K. The comparison reveals a strong impact of the temperature on the dielectric permittivity change under bias electric field and AC signal. Thus, the dielectric tunability was calculated as a function of the temperature from the temperature-dependent dielectric hysteresis loops and is shown in Figure 2d for different AC signals. The dielectric tunability increases from 206% to an extraordinarily high value of 373% as the AC signal is increased from 1 to 20 V. Besides the strong enhancement of the dielectric tunability, the temperature of the dielectric tunability maximum is shifted from ≈ 395 to ≈ 388 K as the AC signal increases from 1 to 20 V. Furthermore, the figure of merit of the maximum dielectric tunability at various AC signals was calculated and is depicted in Figure 2e. It exhibits an exceptionally high value of $\approx 6870\%$ at

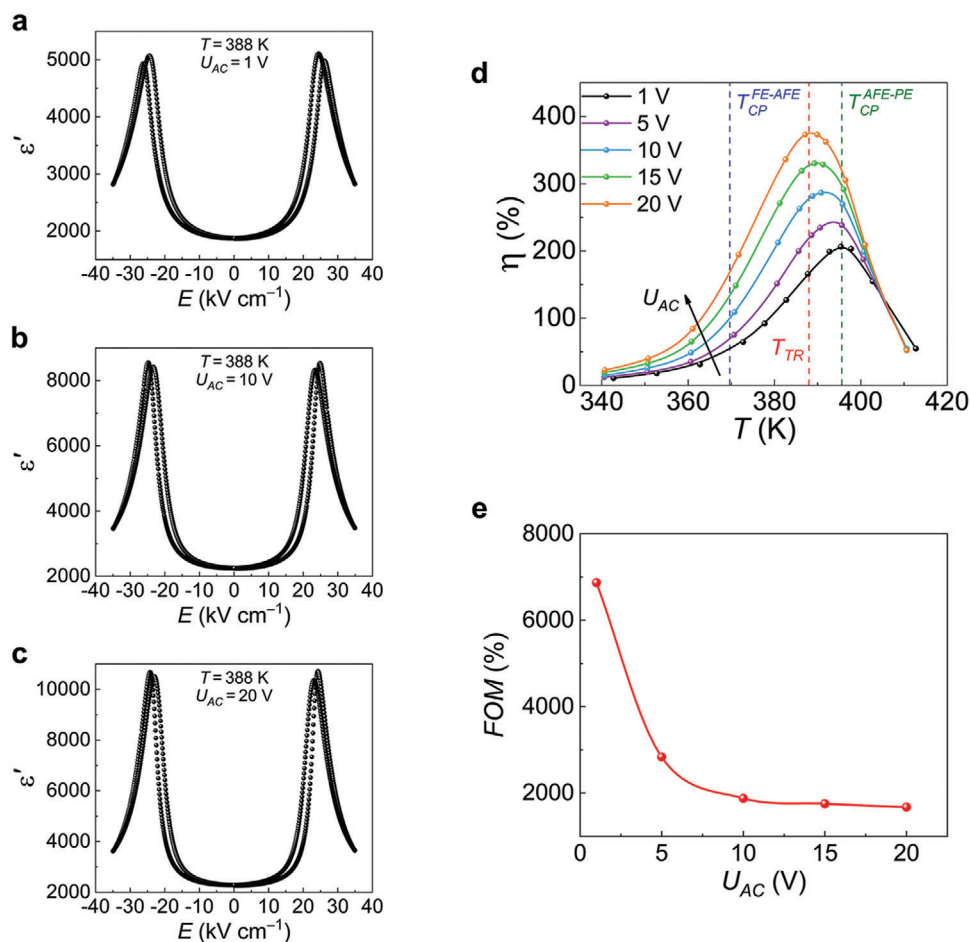


Figure 2. a–c) Electric field dependence of the dielectric permittivity measured with 1, 10, and 20 V AC signal, respectively, during the second measurement loop. d) Dielectric tunability as a function of temperature measured at different AC signals. Vertical lines from left to right represent temperatures of the FE-AFE critical end point, coexistence/triple point, and AFE-PE critical end point, respectively. e) Figure of merit (*FOM*) as a function of AC signal calculated at the temperature of the maximum value of the dielectric tunability.

1 V AC signal. The *FOM* value decreases with increasing AC signal which can be explained by the increase of the dielectric losses. Despite the decrease of the *FOM* value with the AC signal, it still exhibits an extremely high value of $\approx 1680\%$ at 20 V.

In a recent study, the maximum dielectric tunability obtained at 1 V AC signal was associated with the proximity of the field-induced AFE-PE critical end point and the flattening of the free energy potential minimum. Furthermore, it has been demonstrated that the FE-AFE and AFE-PE phase transition temperatures in the antiferroelectric PNZST ceramics are strongly electric field-dependent.^[19] The electric field-temperature phase diagram determined from the dielectric measurement demonstrates the presence of the electric field-induced triple point (see Figure S5, Supporting Information) in the antiferroelectric PNZST ceramics. The coexistence of different phases requires the degeneration of their free energy. Phenomenological Landau theory predicts a strong reduction of the anisotropic free energy in ferroelectrics at the triple point.^[33] According to the classical domain theory, the reduction of the anisotropic free energy in ferroelectrics manifests itself in the decrease in the domain size.^[33,34] In the vicinity of the triple point, the anisotropic

energy approaches zero, which reduces domain size to sub-nanometer dimensions, which was also experimentally observed in ferroelectrics.^[35,36] Hence, a reduction of the anisotropic energy and minimization of the domain structure is also expected at the field-induced triple point in the antiferroelectric PNZST ceramics. In addition, the minimization of the domain size leads to an increase in the domain density, and, consequently, it may result in increased non-linear or extrinsic contribution to the dielectric tunability. The proposed enhancement mechanism is schematically illustrated in **Figure 3a**.

To reveal the role of the domain contribution to the enhancement of the dielectric tunability in antiferroelectric PNZST ceramics, Rayleigh analysis of the dielectric response as a function of the AC signal was conducted. Rayleigh law is used in ferroelectrics to determine the reversible and irreversible contribution of the interface motion to the piezoelectric and dielectric properties.^[20,21,37,38] Figure 3b shows AC voltage signal dependency of the dielectric permittivity at 370 K. For the bias electric fields below 15 kV cm^{-1} , the AC voltage signal has a nearly negligible impact on the dielectric permittivity, however, above 15 kV cm^{-1} , a significant increase of ϵ' with the applied AC

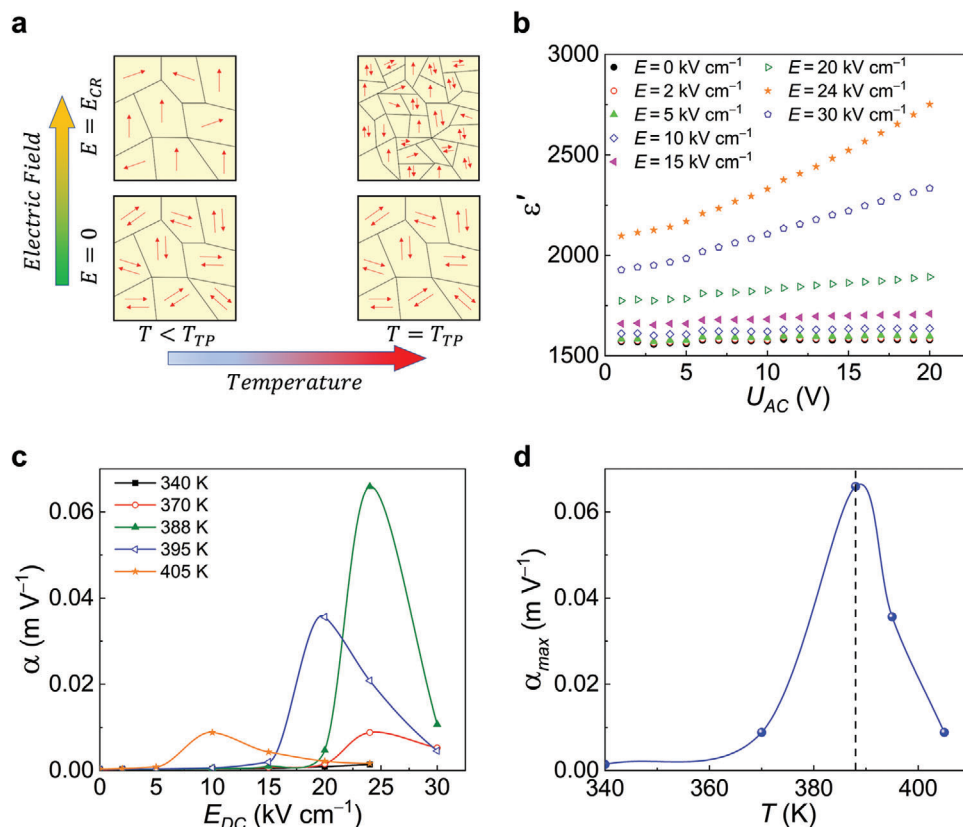


Figure 3. a) Illustration of the electric field evolution of the domain structure below and at the triple point. b) Dielectric permittivity as a function of the amplitude of the AC signal measured at 370 K and different DC electric fields. c) Irreversible Rayleigh coefficient as a function of DC electric field measured at several different temperatures. d) Temperature-dependent maximum value of the irreversible Rayleigh coefficient.

signal is observed. The highest dielectric permittivity change was observed at 24 kV cm⁻¹, which is just below the critical electric field of the field-induced AFE-FE phase transition of the presented temperature (see Figure 3b). At the electric field of 30 kV cm⁻¹, i.e., above the field-induced AFE-FE phase transition, the dielectric permittivity change decreases with the AC voltage signal. The decrease can be attributed to the stabilization of the FE phase and alignment of the FE domains with the electric field. The Rayleigh analysis of the dielectric response as a function of the AC signal provides information on the non-linear contribution to the dielectric response. The irreversible Rayleigh coefficient, α , is typically used to represent the measure of the contribution of the irreversible domain wall or, more generally, interface displacements.^[39] Figure 3c depicts this coefficient as a function of the electric field at several different temperatures. The Rayleigh coefficient exhibits nearly the same behavior for all temperatures. At low electric fields, the irreversible Rayleigh coefficient is small, which implies low irreversible domain dynamics. With increasing electric field, the coefficient increases and reaches a maximum value in the vicinity of the critical electric field which induces the AFE-FE phase transition. Concomitantly with the phase transition, the alignment of FE domains occurs, which decreases the irreversible coefficient and domain contribution to the dielectric response in the FE phase. The increase of the irreversible Rayleigh coefficient with an electric field suggests an increased irreversible domain wall contribution^[40] to the dielec-

tric response in the antiferroelectric phase. The Rayleigh analysis was undertaken at various temperatures, and for each temperature, the maximum non-linear Rayleigh coefficient, α_{max} , was found close to the critical electric field of the AFE-FE phase transition. Figure 3d shows the maximum Rayleigh coefficient as a function of the temperature. The highest Rayleigh coefficient was obtained at 388 K which coincides with the temperature of the triple point found in antiferroelectric PNZST ceramics.^[19] This can be explained along with the minimization of domain size and increase of the domain density.

Furthermore, the PFM measurements at 333 and 388 K were performed and are depicted in Figure 4. At the temperature of 333 K, a classical AFE-FE first-order phase transition occurs. Ferroelectric domain structures emerge in the region where DC voltage of 70 V was applied locally on the samples surface. The micrometer-sized lamellar domains are highlighted in the insets of the panel (a) in Figure 4 (blue arrows). On the other hand, the temperature of 388 K corresponds to the triple point temperature. The amplitude and phase of the PFM response exhibit a nanodomain pattern. Despite the application of a DC voltage of 140 V, twice that which was applied previously, the micro-sized domains are not formed. The sub-micro-sized irregularly shaped domain pattern (marked by white arrows in Figure 4b) resembles a relaxor-like nanodomain response previously observed in relaxor materials by PFM.^[41,42] While some rare lamellar domains were visible, they were small, sub-micron in size. The decrease

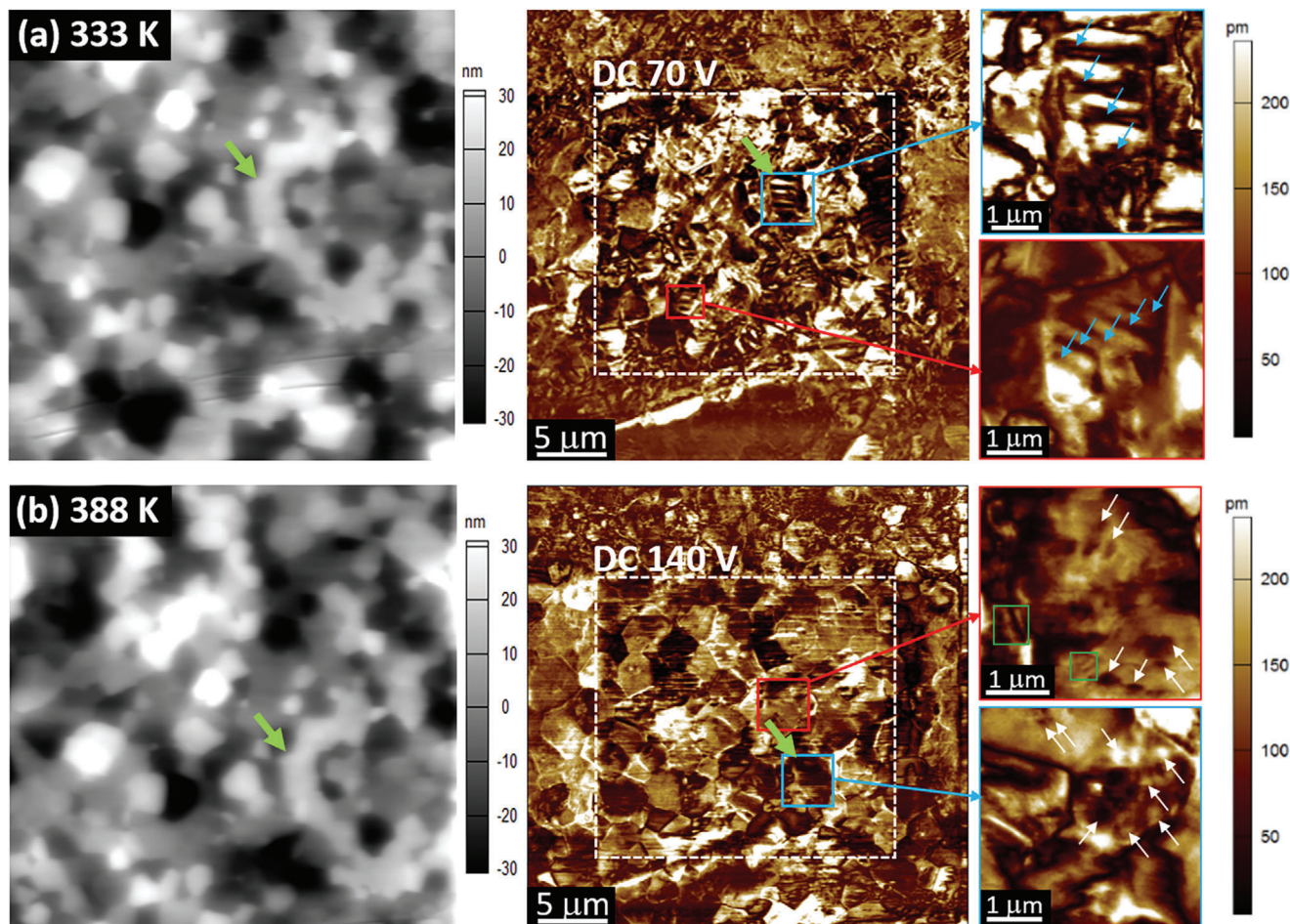


Figure 4. AFM topography and PFM out-of-plane amplitude images were scanned at a) 333 K and b) 388 K. The green arrow in the AFM and PFM images points to the same area. White dashed squares indicate regions where DC electric fields were previously applied. Insets within (a) and (b) display PFM amplitude images of smaller areas denoted by blue and red solid squares. The blue solid square represents the same measurement area. Micrometer-large lamellar domains are highlighted by blue arrows in the insets of the panel (a). The sub-micron-sized irregularly shaped domains and the sub-micron-sized lamellar domains are marked by white arrows and green squares, respectively, in the insets of the panel (b).

in domain size from 333 to 388 K is apparent, indicating domain fragmentation. Consequently, the PFM findings align with the results from Rayleigh analysis and confirm the presence of the electric field-induced nanodomains at the triple point of the antiferroelectric PNZST ceramics.

3. Conclusion

In summary, the mechanism of the dielectric enhancement with bias electric field in the antiferroelectric phase of the PNZST ceramics was investigated by the in situ dielectric and thermal measurements, Rayleigh-type analysis, and piezoresponse force microscopy. Exceptionally high values of the dielectric tunability and figure of merit of $\approx 375\%$ and $\approx 6870\%$, respectively, were obtained in the antiferroelectric phase. It was shown that the increase of the dielectric permittivity with increasing electric field is due to the increased contribution of the non-linear processes, most likely due to the domain wall displacements. This was corroborated by the Rayleigh analysis which revealed an increase of the irreversible contribution in the vicinity of the

AFE-FE phase transition. Furthermore, the extreme value of the dielectric tunability around the triple point was attributed to the minimization of the domain sizes, revealed by the PFM imaging, and concomitantly increased irreversible domain wall contributions to the dielectric permittivity. The results suggest that tailoring of the domain structure is a successful approach to tune the functional properties of not only ferroelectric but also antiferroelectric ceramics. The new understanding of the dielectric tunability in antiferroelectric materials opens additional possibilities to develop and improve the properties of DC-link, snubber, and filter capacitors.

4. Experimental Section

The preparation of the AFE ceramics with a chemical formula $\text{Pb}_{0.99}\text{Nb}_{0.02}[(\text{Zr}_{0.57}\text{Sn}_{0.43})_{0.92}\text{Ti}_{0.08}]_{0.98}\text{O}_3$ (abbreviated as PNZST) is described elsewhere.^[27] The ceramic sample with a thickness of 235 μm was covered with sputtered gold electrodes with a diameter of 1.5 mm on the sample's planar surfaces. Two thin copper wires were attached with a silver paste to provide electrical contacts. A miniaturized NTC

thermistor of 500 k Ω was attached to the sample for sample temperature measurements. The dielectric response and sample temperature were measured simultaneously as a function of the electric field at various fixed temperatures. The sample was first heated to 430 K for 15 min to avoid any possible history-dependent effects of previous measurements and then cooled and stabilized at the measured temperature within ± 2 mK. During the measurement, the electric field was linearly cycled with a frequency of 1 mHz between ± 35 kV cm $^{-1}$. The dielectric hysteresis loops were measured with superimposed AC signals in the 1–20 V range at a frequency of 10 kHz using a precision LCR meter (E4980A, Keysight Technologies, Inc). The values of the real part of the dielectric constant, i.e., the dielectric permittivity ϵ' , and the values of the imaginary part of the dielectric constant, ϵ'' , were calculated from the actual measured quantities, the capacitance C and electrical conductivity G via $\epsilon' = (Cd)/(\epsilon_0 S)$ and $2\pi\nu\epsilon'' = (Gd)/(\epsilon_0 S)$, where ν is the measurement frequency, d is the sample thickness, S is the electrode area, and $\epsilon_0 = 8.85 \times 10^{-12}$ As (Vm) $^{-1}$ is the permittivity of free space. The sample temperature was measured using a high-performance digital multimeter (Keithley 2002, Tektronix, Inc.).

To investigate the domain contribution, the dielectric response was measured under different DC electric fields to which the AC field was superimposed and swept between 1 and 20 V (corresponding to electric field range 0.04–0.85 kV cm $^{-1}$) at several temperatures. The dielectric permittivity was plotted as a function of the AC signal to differentiate extrinsic from intrinsic contributions to the dielectric response by employing the Rayleigh law:

$$\epsilon' = \epsilon'_{int} + \alpha E_0 \quad (3)$$

where, ϵ'_{int} is the reversible Rayleigh coefficient, α is the irreversible Rayleigh coefficient, and E_0 is the amplitude of the AC electric field. By repeating the measurement under different DC electric fields and temperatures, electric field-dependent responses of α and the temperature-dependent response of maximum irreversible Rayleigh coefficient, α_{max} were determined.

The samples were investigated with an atomic force microscope (AFM; Molecular Force Probe 3D, Asylum Research, Santa Barbara, California, USA) equipped with a piezoresponse force microscopy (PFM) module. The images were scanned in dual AC resonance-tracking (DART) vertical mode. Before scanning, the sample was tinned to 45 μ m to ensure good thermal equilibrium during the high-temperature PFM measurements. After that, the sample was polished on fabric using a polishing paste with a gradual decrease in the size of the diamond abrasive down to 0.25 μ m and fine-polished with a colloidal SiO $_2$ suspension as described in ref. [43]. For the PFM scanning, Pt-coated silicon tips with a radius of curvature ≈ 10 nm (OMCL-AC240TM-R3, Olympus, Japan) were used. PFM measurements were performed at 333 and 388 K using a homemade high-temperature set-up with a commercial heater (PolyHeater, Asylum Research, Santa Barbara, California, USA). Prior to each measurement, the sample was heated to 423 K for 10 min. First, an area of 20 \times 20 μ m was scanned using a DC tip voltage of 70 or 140 V. After that, a 35 \times 35 μ m scan was performed with a drive amplitude of 5 V, a frequency of 300 kHz, and a DC tip voltage of 0 V, followed by a few μ m large scans of selected regions at similar voltage.

Supporting Information

Supporting Information is available from the Wiley Online Library or from the author.

Acknowledgements

The authors thank Jena Cilenšek, Katerina Spanou (Erasmus+ programme), Val Fišinger, and Brigita Kmet for the laboratory assistance. The authors acknowledge fruitful discussions with Prof. Hana Uršič on the interpretation of PFM results. This research was funded by the Slovenian Research and Innovation Agency under Projects Nos. J2-4464, N2-0212, and Programs Nos. P1-0125, P2-0105.

Conflict of Interest

The authors declare no conflict of interest.

Data Availability Statement

The data that support the findings of this study are available from the corresponding author upon reasonable request.

Keywords

antiferroelectrics, dielectric tunability, non-linear contributions

Received: July 17, 2024
Revised: September 3, 2024
Published online: October 4, 2024

- [1] L. B. Kong, S. Li, T. S. Zhang, J. W. Zhai, F. Y. C. Boey, J. Ma, *Prog. Mater. Sci.* **2010**, *55*, 840.
- [2] S. Kwon, W. Hackenberger, E. Alberta, E. Furman, M. Lanagan, *IEEE Electr. Insul. Mag.* **2011**, *27*, 43.
- [3] F. Li, H. Zhang, H. Luo, M. Xing, L. Cao, C. Wu, Y. Zou, D. Jia, Y. Zhou, Y. Huang, H. Ke, *Adv. Electron. Mater.* **2023**, *9*, 2201243.
- [4] V. O. Sherman, A. K. Tagantsev, N. Setter, D. Iddles, T. Price, *J. Appl. Phys.* **2006**, *99*, 074104.
- [5] A. K. Tagantsev, V. O. Sherman, K. F. Astafiev, J. Venkatesh, N. Setter, *J. Electroceramics.* **2003**, *11*, 5.
- [6] G. F. Engel, presented at CIPS 2016; 9th Int. Conf. on Integrated Power Electronics Systems, Nuremberg, Germany **2016**, pp. 1–7.
- [7] C. A. Randall, Z. Fan, I. Reaney, L.-Q. Chen, S. Trolier-McKinstry, *J. Am. Ceram. Soc.* **2021**, *104*, 3775.
- [8] M. Hoffmann, Z. Wang, N. Tasneem, A. Zubair, P. V. Ravindran, M. Tian, A. A. Gaskell, D. Triyoso, S. Consiglio, K. Tapily, R. Clark, J. Hur, S. S. K. Pentapati, S. K. Lim, M. Dopita, S. Yu, W. Chern, J. Kacher, S. E. Reyes-Lillo, D. Antoniadis, J. Ravichandran, S. Slesazek, T. Mikolajick, A. I. Khan, *Nat. Commun.* **2022**, *13*, 1228.
- [9] L. Li, M. Spreitzer, D. Suvorov, X. M. Chen, *J. Appl. Phys.* **2016**, *120*, 074109.
- [10] R. Pirc, B. Rožič, J. Koruza, B. Malič, Z. Kutnjak, *Europhys. Lett.* **2014**, *107*, 17002.
- [11] J. Frederick, X. Tan, W. Jo, *J. Am. Ceram. Soc.* **2011**, *94*, 1149.
- [12] Y. Liu, X. Lu, Y. Jin, S. Peng, F. Huang, Y. Kan, T. Xu, K. Min, J. Zhu, *Appl. Phys. Lett.* **2012**, *100*, 212902.
- [13] B. Peng, H. Fan, Q. Zhang, *J. Am. Ceram. Soc.* **2013**, *96*, 1852.
- [14] J. Wang, T. Yang, K. Wei, G. Li, S. Chen, *J. Am. Ceram. Soc.* **2012**, *95*, 1483.
- [15] J. Wang, T. Yang, S. Chen, X. Yao, A. Peláiz-Barranco, *J. Alloys Compd.* **2014**, *587*, 827.
- [16] T. Sa, N. Qin, G. Yang, D. Bao, *Appl. Phys. Lett.* **2013**, *102*, 172906.
- [17] L. Li, M. Spreitzer, D. Suvorov, *Appl. Phys. Lett.* **2014**, *104*, 182902.
- [18] H. Pan, Z. Tian, M. Acharya, X. Huang, P. Kavle, H. Zhang, L. Wu, D. Chen, J. Carroll, R. Scales, C. J. G. Meyers, K. Coleman, B. Hanrahan, J. E. Spanier, L. W. Martin, *Adv. Mater.* **2023**, *35*, 2300257.
- [19] V. Jurečič, L. Fulanović, J. Koruza, V. Bobnar, N. Novak, *Phys. Rev. Mater.* **2023**, *7*, 114407.
- [20] N. Bassiri-Gharb, I. Fujii, E. Hong, S. Trolier-McKinstry, D. V. Taylor, D. Damjanovic, *J. Electroceramics.* **2007**, *19*, 49.
- [21] D. A. Hall, *J. Mater. Sci.* **2001**, *36*, 4575.
- [22] H. Dederichs, G. Arlt, *Ferroelectrics.* **1986**, *68*, 281.
- [23] D. A. Hall, M. M. Ben-Omran, *J. Phys. Condens. Matter.* **1998**, *10*, 9129.
- [24] J. M. Worlock, P. A. Fleury, *Phys. Rev. Lett.* **1967**, *19*, 1176.

- [25] H. He, X. Tan, *Phys. Rev. B* **2005**, 72, 024102.
- [26] S. B. Vakhrushev, D. Andronikova, I. Bronwald, E. Yu Koroleva, D. Chernyshov, A. V. Filimonov, S. A. Udovenko, A. I. Rudskoy, D. Ishikawa, A. Q. R. Baron, A. Bosak, I. N. Leontiev, A. K. Tagantsev, *Phys. Rev. B* **2021**, 103, 214108.
- [27] X. Tan, S. E. Young, Y. H. Seo, J. Y. Zhang, W. Hong, K. G. Webber, *Acta Mater.* **2014**, 62, 114.
- [28] N. Novak, F. Weyland, S. Patel, H. Guo, X. Tan, J. Rödel, J. Koruza, *Phys. Rev. B* **2018**, 97, 094113.
- [29] B. Lewis, *Proc. Phys. Soc.* **1959**, 73, 17.
- [30] A. Bradeško, A. Hedl, L. Fulanović, N. Novak, T. Rojac, *APL Mater.* **2019**, 7, 071111.
- [31] T. Jiao, C. You, N. Tian, L. Ma, Z. Duan, F. Yan, P. Ren, G. Zhao, *J. Eur. Ceram. Soc.* **2022**, 42, 4926.
- [32] R. Li, D. Xu, C. Du, Q. Ma, F. Zhang, X. Liang, D. Wang, Z. Shi, W. Liu, D. Zhou, *Nat. Commun.* **2024**, 15, 3754.
- [33] A. A. Heitmann, G. A. Rossetti Jr., *J. Am. Ceram. Soc.* **2014**, 97, 1661.
- [34] M. E. Lines, A. M. Glass, in *Principles and Applications of Ferroelectrics and Related Materials*, Oxford University Press, Oxford **2001**.
- [35] D. I. Woodward, J. Knudsen, I. M. Reaney, *Phys. Rev. B* **2005**, 72, 104110.
- [36] J. Gao, D. Xue, Y. Wang, D. Wang, L. Zhang, H. Wu, S. Guo, H. Bao, C. Zhou, W. Liu, S. Hou, G. Xiao, X. Ren, *Appl. Phys. Lett.* **2011**, 99, 092901.
- [37] L. M. Riemer, L. Jin, H. Uršič, M. Otonicar, T. Rojac, D. Damjanovic, *J. Appl. Phys.* **2021**, 129, 054101.
- [38] D. V. Taylor, D. Damjanovic, *J. Appl. Phys.* **1997**, 82, 1973.
- [39] Z. Luo, X. Lou, F. Zhang, Y. Liu, D. Chang, C. Liu, Q. Liu, B. Dkhil, M. Zhang, X. Ren, H. He, *Appl. Phys. Lett.* **2014**, 104, 142904.
- [40] D. Damjanovic, M. Demartin, *J. Phys. Condens. Matter* **1997**, 9, 4943.
- [41] V. V. Shvartsman, A. L. Kholkin, A. Orlova, D. Kiselev, A. A. Bogomolov, A. Sternberg, *Appl. Phys. Lett.* **2005**, 86, 202907.
- [42] H. Ursic, S. Drnovsek, B. Malic, *J. Phys. Appl. Phys.* **2016**, 49, 115304.
- [43] H. Uršič, U. Prah, *Proc. R. Soc. Math. Phys. Eng. Sci.* **2019**, 475, 20180782.